Inorg. Chem. **2007**, *46*, 2725–2734

Construction of Robust Open Metal–Organic Frameworks with Chiral Channels and Permanent Porosity

Daofeng Sun, Yanxiong Ke,[†] David J. Collins, Gary A. Lorigan, and Hong-Cai Zhou*

Department of Chemistry and Biochemistry, Miami University, Oxford, Ohio 45056

Received December 27, 2006

Four new metal–organic frameworks (MOFs) containing chiral channels have been synthesized using an achiral, triazine-based trigonal-planar ligand, 4,4′,4″-*s*-triazine-2,4,6-triyltribenzoate (TATB), and an hourglass secondary building unit (SBU): $Zn_3(TATB)_2(H_2O)_2 \cdot 4DMF \cdot 6H_2O$ (**1**); $Cd_3(TATB)_2(H_2O)_2 \cdot 7DMA \cdot 10H_2O$ (**2**); $[H_2N(CH_3)_2][Zn_3(TATB)_2(HCOO)] \cdot HN(CH_3)_2 \cdot 3DMF \cdot 3H_2O$ (**3**); $[H_2N(CH_3)_2][Cd_3(TATB)_2(CH_3COO)] \cdot HN(CH_3)_2 \cdot 3DMA \cdot 4H_2O$ (**4**). MOFs **1** and **2** are isostructural and possess (10,3)-a nets containing large chiral channels of 20.93 and 21.23 Å, respectively, but are thermally unstable due to the easy removal of coordinated water molecules on the SBU. Replacement of these water molecules by formate or acetate generated in situ leads to **3** and **4**, respectively. Formate or acetate links SBUs to form infinite helical chains bridged by TATB to create three-dimensional anionic networks, in which one of the two oxygen atoms of the formate or acetate is uncoordinated and points into the void of the channels. This novel SBU-stabilization and channel-functionalization strategy may have general implications in the preparation of new MOFs. Thermogravimetric analysis (TGA) shows that solvent-free **3′** is thermally stable to 410 °C, while TGA studies on samples vapor-diffused with water, methanol, and chloroform show reversible adsorption. MOF **3** also has permanent porosity with a large Langmuir surface area of 1558 m^2/g. All complexes exhibit similar strong luminescence with a λ_{max} of approximately 423 nm upon excitation at 268.5 nm.

Porous metal−organic frameworks (MOFs) containing chiral channels have gained considerable attention in recent years due to their potential applications, most notably enantioselective separation and catalysis.[1,2] Chiral MOFs have been constructed using chiral ligands[3] or with templating by chiral molecules.[2a] For instance, Lin and co-workers have reported a series of chiral MOFs based on chiral organic ligands.[4] Rosseinsky and co-workers have synthesized a number of chiral MOFs by using chiral coligands.[5] However, examples of MOFs containing chiral channels possessing both high thermal stability and porosity are rare.

One of the most common ligands in MOF syntheses is benzenetricarboxylate (BTC; see Supporting Information, Scheme S1), which has been used to construct MOFs containing chiral channels.[6,7] Interpenetration in these structures results in stable frameworks but limits pore size. Recently, we reported three isostructural Mn, Co, and Zn MOFs based on 4,4′,4″-*s*-triazine-2,4,6-triyl-tribenzoate (TATB) containing large tetrahedral cages with high thermal stability.[8] In these compounds, all the TATB ligands are planar; there exists strong $\pi-\pi$ interaction between adjacent

* To whom correspondence should be addressed. E-mail: zhouh@muohio.edu.

[†] Current address: East China University of Science and Technology.

(1) (a) Abrahams, B. F.; Jackson, P. A.; Robson, R. *Angew. Chem., Int. Ed.* **1998**, *37*, 2656. (b) Abrahams, B. F.; Moylan, M.; Orchard, S. D.; Robson, R. *Angew. Chem., Int. Ed.* **2003**, *42*, 1848. (c) Dincá, M.; Long, J. R. *J. Am. Chem. Soc.* **2005**, *127*, 9376. (d) Fan, Q.-H.; Ren, C.-Y.; Yeung, C.-H.; Hu, W.-H.; Chan, A. S. C. *J. Am. Chem. Soc.* **1999**, *121*, 7407. (e) Sundarababu, G.; Leibovitch, M.; Corbin, D. R.; Scheffer, J. R.; Ramamurthy, V. *Chem. Commun.* **1996**, 2159. (f) Verbiest, T.; van Elshocht, S.; Karuanen, M.; Hellemans, L.; Snauwaert, J.; Nuckolls, C.; Katz, T. J.; Persoons, A. *Science* **1998**, *282*, 913. (g) Kesanli, B.; Lin, W. *Coord. Chem. Rev.* **2003**, *246*, 305. (h) Zeng, M. H.; Wang, B.; Wang, X.-Y.; Zhang, W.-X.; Chen, X.-M.; Gao, S. *Inorg. Chem.* **2006**, *45*, 7069. (i) Tang, Y.-Z.; Huang, X.-F.; Song, Y.-M.; Chan, P. W. H.; Xiong, R. G. *Inorg. Chem.* **2006**, *45*, 4868. (j) Barbour, L. J. *Chem. Commun.* **2006**, 1163.

(2) (a) Bradshaw, D.; Prior, T. J.; Cussen, E. J.; Claridge, J. B.; Rosseinsky, M. J. *J. Am. Chem. Soc.* **2004**, *126*, 6106. (b) Gu, X.; Xue, D. *Inorg. Chem.* **2006**, *45*, 9257.

(3) Wu, C.-D.; Hu, A.; Zhang, L.; Lin, W. *J. Am. Chem. Soc.* **2005**, *127*, 8940.

(4) Lin, W. *J. Solid State Chem.* **2005**, *178*, 2486.

(5) Bradshaw, D.; Claridge, J. B.; Cussen, E. J.; Prior, T. J.; Rosseinsky, M. J. *Acc. Chem. Res.* **2005**, *38*, 273.

(6) (a) Kepert, C. J.; Prior, T. J.; Rosseinsky, M. J. *J. Am. Chem. Soc.* **2000**, *122*, 5158. (b) Prior, T. J.; Rosseinsky, M. J. *Inorg. Chem.* **2003**, *42*, 1564.

(7) O'Keeffe, M.; Eddaoudi, M.; Li, H.; Reinek, T.; Yaghi, O. M. *J. Solid State Chem.* **2000**, *152*, 3.

(8) Sun, D.; Ma, S.; Ke, Y.; Petersen, T. M.; Zhou, H.-C. *Chem. Commun.* **2005**, 2663.

10.1021/ic0624773 CCC: $37.00
Published on Web 03/10/2007

ligands. This is fundamentally different from the structurally similar BTB ligand first reported by Yaghi,[9] which is nonplanar because of the repulsion between the hydrogen atoms of the central ring and those of peripheral rings. TATB should rather be considered an extension of BTC since both are trigonal planar; this makes it possible to construct open MOFs containing chiral channels using TATB because the (10,3)-a net, which contains chiral channels, is a common structural type for BTC-containing MOFs.[5] We have demonstrated earlier via photoluminescence and mass spectrometry studies that the trigonal-planar ligand *s*-heptazine tribenzoate (HTB) forms ligand dimers ("Piedfort units") and that the combination of three of these ligand pairs with a trizinc "hourglass" SBU gives rise to a (10,3)-a MOF with large chiral channels.[10] We have also shown that a microporous MOF containing TATB Piedfort units and dicopper paddlewheel SBUs exhibits high H_2 uptake.[11a] Most recently, we have reported another MOF constructed using TATB Piedfort units and hemoglobin-like SBUs possessing high gas adsorption affinity.[11b] Herein we describe the syntheses and characterization of four MOFs containing chiral channels created using TATB ligand pairs and an hourglass SBU: $Zn_3(TATB)_2(H_2O)_2 \cdot 4DMF \cdot 6H_2O$ (**1**); $Cd_3(TATB)_2(H_2O)_2 \cdot 7DMA \cdot 10H_2O$ (**2**); $[H_2N(CH_3)_2][Zn_3(TATB)_2(HCOO)] \cdot [HN(CH_3)_2] \cdot 3DMF \cdot 3H_2O$ (**3**); $[H_2N(CH_3)_2][Cd_3(TATB)_2(CH_3COO)] \cdot [HN(CH_3)_2] \cdot 3DMA \cdot 4H_2O$ (**4**). Compounds **1** and **2** are three-dimensional open MOFs containing large chiral channels and possessing the (10,3)-a net topology. Compounds **3** and **4**, which have high thermal stability while retaining significant porosity, can be considered derivatives of **1** and **2**.

Experimental Section

Commercially available reagents were used as received without further purification. Infrared spectra were obtained on a Perkin-Elmer Spectrum One FT-IR with a universal diamond ATR sampling accessory in the 650−4000 cm^{-1} region. Elemental analyses (C, H, and N) were performed by Canadian Microanalytical Service, Ltd. Thermogravimetric analysis (TGA) was performed under N_2 on a Perkin-Elmer TGA 7, and a Beckman Coulter SA3100 surface area analyzer was used to measure gas adsorption. XRPD patterns were obtained on a Scintag X1 powder diffractometer system using Cu Kα radiation with a variable divergent slit, solid-state detector and a routine power of 1400 W (40 kV, 35 mA). Powder samples were dispersed on low-background quartz XRD slides (Gem Depot, Inc., Pittsburgh, PA) for analyses. H_3TATB was synthesized according to previously published methods.[11] Solvothermal reaction mixtures were heated from room temperature to the desired temperature at a rate of 1.0 °C/min and cooled at a rate of 0.1 °C/min.

Synthesis of $Zn_3(TATB)_2(H_2O)_2 \cdot 4DMF \cdot 6H_2O$ (1). H_3TATB (0.005 g, 0.0113 mmol) and $Zn(NO_3)_2 \cdot 6H_2O$ (0.025 g, 0.085 mmol) were dissolved in DMF (*N*,*N*-dimethylformamide, 1.5 mL) and sealed in a Pyrex tube under vacuum. The tube was held at 90 °C for 3 days to produce colorless block crystals. The crude product was washed with DMF to give pure **1** (0.005 g, 0.003 mmol, yield 60% based on TATB). Anal. Calcd for $C_{60}H_{68}N_{10}O_{24}Zn_3$: C, 47.74; H, 4.54; N, 9.28. Found: C, 47.87; H, 4.54; N, 9.42. IR (cm^{-1}): 3448 (w, br), 2931 (w), 1660 (vs), 1568 (s), 1505 (s), 1383 (vs), 1354 (vs), 1091 (s), 820 (m), 776 (vs), 659 (m).

Synthesis of $Cd_3(TATB)_2(H_2O)_2 \cdot 7DMA \cdot 10H_2O$ (2). H_3TATB (0.005 g, 0.0113 mmol) and $Cd(NO_3)_2 \cdot 4H_2O$ (0.025 g, 0.081 mmol) were dissolved in DMA (*N*,*N*-dimethylacetamide, 1.5 mL) and sealed in a Pyrex tube under vacuum. The tube was held at 120 °C for 24 h to produce colorless block crystals. The crude product was washed with DMA to give pure **2** (0.007 g, 0.003 mmol, yield 64% based on H_3TATB). Accurate elemental analysis was difficult to obtain due to high porosity and poor stability of the sample; the formula of **2** was established through TGA and X-ray crystallography. IR (cm^{-1}): 3278 (w, br), 1595 (m), 1538 (m), 1505 (s), 1377 (vs), 1352 (vs), 1016 (m), 820 (m), 773 (vs), 699 (m).

Synthesis of $[H_2N(CH_3)_2][Zn_3(TATB)_2(HCOO)] \cdot HN(CH_3)_2 \cdot 3DMF \cdot 3H_2O$ (3). H_3TATB (0.005 g, 0.0113 mmol), $Zn(NO_3)_2 \cdot 6H_2O$ (0.025 g, 0.084 mmol), and HBF_4 (0.025 mL) in DMF (1.5 mL) was sealed in a Pyrex tube under vacuum. The tube was held at 120 °C for 24 h to produce colorless, rodlike crystals. The crude product was washed with DMF to give pure **3** (0.0035 g, 0.002 mmol, yield 43% based on H_3TATB). Anal. Calcd for $C_{62}H_{67}N_{11}O_{20}Zn_3$: C, 50.23; H, 4.56; N, 10.39. Found: C, 50.84; H, 4.78; N, 10.66. IR (cm^{-1}): 2931 (w, br), 1655 (m), 1563 (m), 1504 (s), 1381 (s), 1352 (vs), 1095 (m), 1016 (m), 821 (s), 774 (vs), 699 (m).

Synthesis of $[H_2N(CH_3)_2][Cd_3(TATB)_2(CH_3COO)] \cdot HN(CH_3)_2 \cdot 3DMA \cdot 4H_2O$ (4). H_3TATB (0.005 g, 0.0113 mmol), $Cd(NO_3)_2 \cdot 4H_2O$ (0.024 g, 0.078 mmol), and HBF_4 (0.025 mL) in DMA (1.5 mL) was sealed in a Pyrex tube under vacuum. The tube was held at 120 °C for 36 h to produce colorless, rodlike crystals. The crude product was washed with DMA to give pure **4** (0.003 g, 0.002 mmol, yield 32% based on TATB). Anal. Calcd for $Cd_3C_{66}H_{77}N_{11}O_{21}$: C, 46.70; H, 4.57; N, 9.08. Found: C, 45.79; H, 4.15; N, 9.32. IR (cm^{-1}): 3061 (w, br), 1657 (s), 1505 (s), 1379 (s), 1350 (vs), 1015 (m), 881 (m), 830 (m), 772 (vs), 700 (m), 821 (s), 774 (vs), 699 (m).

Gas Adsorption Measurements. Samples of **1** and **3** were soaked in methanol for 5 h, and the extract was discarded. Fresh methanol was subsequently added, and the crystals were allowed to soak for another 24 h. After the removal of methanol by decanting, the samples were dried under dynamic vacuum at 60 °C for 15 h. Before the measurement, the sample was dried again using the "outgas" function of the surface area analyzer for 2 h at 150 °C. Measurements were performed with methane, prepurified N_2, and 99.9995% pure H_2.

Generation of $[H_2N(CH_3)_2][Zn_3(TATB)_2(HCOO)]$ (3′) and 3′·Guest. Samples of **3** were soaked in methanol at room temperature for 1−2 days, and the supernatant was decanted. Crystals were dried under dynamic vacuum at 60 °C for 12 h to produce solvent-free **3′**, confirmed by TGA. These freshly prepared samples were used for vapor diffusion with water, methanol, or chloroform. TGA measurements were performed after 12 h of vapor diffusion.

X-ray Crystallography. Single-crystal X-ray data were collected on a Bruker Smart Apex diffractometer equipped with an Oxford Cryostream low-temperature device and a fine-focus sealed-tube X-ray source (Mo Kα radiation, $\lambda = 0.710\,73$ Å, graphite monochromated) operating at 45 kV and 40 mA. MOFs **1** and **2** easily lose solvates from their channels when exposed to air; these crystals were sealed in thin-wall capillaries with small amounts of

(9) Chen, B. L.; Eddaoudi, M.; Hyde, S. T.; O'Keeffe, M.; Yaghi, O. M. *Science* **2001**, *291*, 1021.
(10) Ke, Y.; Collins, D. J.; Sun, D.; Zhou, H.-C. *Inorg. Chem.* **2006**, *45*, 1897.
(11) (a) Sun, D.; Ma, S.; Ke, Y.; Collins, D. J.; Zhou, H.-C. *J. Am. Chem. Soc.* **2006**, *128*, 3896. (b) Ma, S.; Zhou, H.-C. *J. Am. Chem. Soc.* **2006**, *128*, 11734.

Table 1. Crystal Data for **1**−**4**

param	**1**		**2**	**3**		**4**	
formula	$C_{48}H_{28}N_6O_{14}Zn_3$	$C_{48}H_{28}N_6O_{14}Zn_3$	$C_{48}H_{28}Cd_3N_6O_{14}$	$C_{52}H_{36.5}N_{7.5}O_{14}Zn_3$	$C_{49}H_{29}N_6O_{15.5}Zn_3$	$C_{50}H_{24}Cd_3N_6O_{14}$	$C_{50}H_{24}Cd_3N_6O_{14}$
fw	1108.87	1108.87	1246.93	1186.5	1145.89	1269.95	1269.95
cryst syst	cubic	cubic	cubic	tetragonal	tetragonal	tetragonal	tetragonal
space group	$P4_332$	$P4_132$	$P4_332$	$P4_322$	$P4_122$	$P4_322$	$P4_122$
T, K	213(2)	213(2)	273(2)	213(2)	183(2)	213(2)	213(2)
a, Å	25.6349(2)	25.6415(6)	26.001(3)	17.8737(3)	17.9980(3)	18.0373(4)	18.0494(4)
c, Å				26.2972(7)	25.9577(9)	27.260 (2)	27.170 (2)
α, deg	90	90	90	90	90	90	90
V, Å^3	*16 845.9(2)*	*16 858.9(7)*	*17 578(4)*	*8401.1(3)*	*8408.4(4)*	*8869.0(5)*	*8851.5(5)*
Z	4	4	4	4	4	4	4
ρ_{calc}, g cm^{-3}	0.437	0.437	0.471	0.938	0.905	0.951	0.953
μ, mm^{-1}	0.445	0.444	0.38	0.895	0.894	0.753	0.755
R1, wR2, %	2.8, 4.9	2.56, 4.67	10.46, 27.09	5.3, 18.74	4.53, 16.00	6.02, 19.70	6.31, 18.37
GOF (F^2)	0.787	0.765	1.112	1.107	1.113	1.181	1.185
Flack param	0.01(1)	0.04(1)	0.1(2)	−0.01(2)	−0.03(2)	−0.06(6)	−0.04(6)

mother liquor. Frames were collected with 0.3° intervals in φ and ω for 45 s/frame such that a hemisphere of data was collected. Raw data collection and refinement were done using SMART; data reduction was performed using SAINT+ and corrected for Lorentz and polarization effects; absorption corrections were applied using the SADABS routine.[12] The structure was solved by direct methods and refined by full-matrix least squares on F^2 using SHELX-97.[13] Non-hydrogen atoms were refined with anisotropic displacement parameters during the final cycles. Hydrogen atoms on carbon were calculated in ideal positions with isotropic displacement parameters set to $1.2U_{eq}$ of the attached atom. In all cases, solvent molecules were highly disordered, and attempts to locate and refine the solvent peaks were unsuccessful; contributions to scattering due to these solvent molecules were removed using the SQUEEZE routine of PLATON and refined further using the data generated.[14] The best of several datasets for **2** was used for structural solution and refinement. Crystal data for all compounds are summarized in Table 1.

X-ray Powder Diffraction (XRPD). A freshly prepared sample of **3** was heated to 150, 250, and 370 °C for 10−30 min; XRPD was collected after 10−30 min at each temperature.

Thermal Stabilities of MOFs 1−4. TGA's of **1**−**4** were used to determine thermal stabilities.

NMR Studies. Solution NMR data were collected on a Bruker 200- or 300-MHz spectrometer, while solid-state NMR spectra were recorded on a Bruker Avance 500-MHz solid-state NMR spectrometer. For the one-dimensional solid-state NMR experiments, the ^{1}H and ^{13}C frequencies were 500.13 and 125.77 MHz, respectively. The experiments were performed using a triple resonance CPMAS probe spinning at 8 kHz. The CPMAS data was collected at different spinning speeds to distinguish real peaks from spinning side bands. A 4.5 μs proton $\pi/2$ pulse was used with a cross polarization contact time of 2 ms. The spectra were collected at 25 °C with a recycle delay of 3 s. The 2D HETCOR (heteronuclear chemical shift correlation) solid-state NMR through-space experiment was performed on H_3TATB. The ^{1}H and ^{13}C frequencies were 500.13 and 125.77 MHz, respectively. The experiment was performed using a triple resonance MAS probe. A 2.5 μs proton $\pi/2$ pulse was used with a cross polarization contact time of 0.5 ms with ^{1}H TPPM decoupling. The relaxation delay was 3 s. The 2D data consisted of 128 experiments with 800 scans for each experiment. The spinning speed was maintained at 14 kHz. Spectral widths of 37 kHz and 26 kHz were used for ^{13}C and ^{1}H, respectively. The 2D data was processed with 10 Hz line broadening and with a size of 1024 in both dimensions. The ^{1}H and ^{13}C chemical shifts were referenced to external TMS.

Photoluminescence Measurements. Photoluminescence spectra were obtained on a Perkin-Elmer LS 50B luminescence spectrometer. The solid samples were suspended in DMF solution. $Ln(NO_3)_3 \cdot 6H_2O$ (Ln = Pr, Nd, Tb, and Yb) and $Cd(NO_3)_2$ were used in the photoluminescene measurement. In general, the nitrate salts were added directly into the DMF solution containing the samples.

Computational Methods. To establish a suitable method using density functional theory (DFT)[15] for determining $\pi-\pi$ interactions in the H_3TATB Piedfort unit, multiple methods were examined using the dimer of the simpler *s*-triazine molecule, $(C_3N_3H_3)_2$ (see Supporting Information). The optimal method from this preliminary study was applied to optimize the structure of H_3TATB; this optimized structure was used to generate the potential energy surface of the H_3TATB Piedfort structure. The HCTH/407 exchange-correlation generalized gradient approximation functional was found to best reproduce the crystalline structure of both the monomer and dimer and was employed throughout.[16] The 6-31G(d,p) basis set was used throughout.[17] Natural bond orbital (NBO)[18] analysis was also performed on the optimized H_3TATB molecule. All calculations were performed using the Gaussian03 program.[19]

Results and Discussion

Computational Evidence of the Piedfort Unit. Derivatives of *s*-triazine and tri-*s*-triazine have found applications in the manufacturing of polymers, dyes, pesticides, and nonlinear optics.[20] In most compounds, $\pi-\pi$ interaction

(12) *SAINT+*, version 6.22; Bruker Analytical X-Ray Systems, Inc.: Madison, WI, 2001.
(13) Sheldrick, G. M. *SHELX-97*; Bruker Analytical X-Ray Systems, Inc.: Madison, WI, 1997.
(14) Spek, A. L. *J. Appl. Crystallogr.* **2003**, *36*, 7.
(15) Parr, R. G.; Yang, W. *Density-functional Theory of Atoms and Molecules*; Oxford University Press: New York, 1989.
(16) Boese, A. D.; Handy, N. C. *J. Chem. Phys.* **2001**, *114*, 5497.
(17) (a) Francl, M. M.; Pietro, W. J.; Hehre, W. J.; Binkley, J. S.; DeFrees, D. J.; Pople, J. A.; Gordon, M. S. *J. Chem. Phys.* **1982**, *77*, 365. (b) Hariharan, P. C.; Pople, J. A. *Theor. Chim. Acta* **1973**, *28*, 213. (c) Hariharan, P. C.; Pople, J. A. *J. Mol. Phys.* **1974**, *27*, 209. (d) Hehre, W. J.; Ditchfield, R.; Pople, J. A. *J. Chem. Phys.* **1972**, *56*, 2257.
(18) (a) Carpenter, J. E.; Weinhold, F. *J. Mol. Struct.* (*Theochem*) **1988**, *196*, 41. (b) Foster, J. P.; Weinhold, F. *J. Am. Chem. Soc.* **1980**, *102*, 7211. (c) Glendening, E. D.; Reed, A. E.; Carpenter, J. E.; Weinhold., F. *NBO*, version 3.1. (d) Reed, A. E.; Curtiss, L. A.; Weinhold, F. *Chem. Rev.* **1988**, *88*, 899. (e) Reed, A. E.; Weinstock, R. B.; Weinhold, F. *J. Chem. Phys.* **1985**, *83*, 735.
(19) Frisch, M. J.; et al. *Gaussian 03*, revision C.02; Gaussian, Inc.: Wallingford, CT, 2004.
(20) (a) Bock, H.; Babeau, A.; Seguy, I.; Jolinat, P.; Destruel, P. *ChemPhysChem* **2002**, *3*, 532. (b) Cho, S. Y.; Chang, Y.; Kim, J. S.; Lee, S. C.; Kim, C. *Macromol. Chem. Phys.* **2001**, *202*, 263.

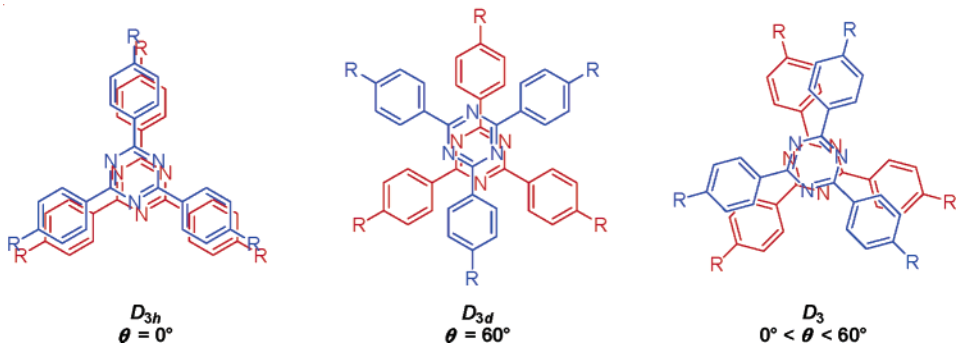

Figure 1. Three possible symmetries of the TATB Piedfort unit.

between triazine rings is typically observed. Unlike benzene rings, which typically interact in more electrostatically favored point-to-face or parallel-displaced arrangements,[21] *s*-triazine rings typically stack in a highly symmetric face-to-face arrangement (see Supporting Information, Figure S1), with both electrostatic attraction and $\pi-\pi$ interaction playing a role. This dimeric face-to-face stacking mode has been nicknamed the "Piedfort unit"[22] and has been described both in triaryloxytriazines[23] and in platinum clusters of tripyridinetriazine.[24] *s*-Triazine dimers can take one of three symmetries, as shown in Figure 1. The D_{3d} dimer maximizes electrostatic interaction between positive carbon atoms and negative nitrogen atoms.

The relative binding energy of the $(H_3TATB)_2$ Piedfort structure was obtained by a potential energy surface scan, with the optimized structure of the H_3TATB molecule frozen. The planar molecules were kept parallel and single-point energies calculated across scans of separation distance (d) and rotational angle (θ). For the potential energy surface for d, the rotational angle between the two molecules was held at 60°. A minimum energy is found at a separation of 3.77 Å (see Supporting Information, Figure S3A). This separation was maintained for the rotational angle scan (Figure S3B). As expected, the lowest energy of the dimer system is located at $\theta = 60°$ (D_{3d} symmetry), with a relative energy (with respect to free molecules) of −6.2 kcal/mol. However, a local minimum is also found at $\theta = 14°$ (D_3 symmetry), with a relative energy of −4.9 kcal/mol. It is likely that this second minimum comes from favorable parallel-displaced interactions between peripheral benzoic acid rings and/or alignment of carboxylate protons. Regardless of the absolute shape of the potential energy surface, it is apparent that interconversion between the various configurations of the dimer has a very low energy barrier (<3 kcal/mol); consequently, all forms, including a chiral D_3 form, are likely to be present in solution.

Mass Spectrometry of Piedfort Unit. Evidence for ligand pairing in solution comes from mass spectrometry. Two peaks are visible at *m*/*z* 440.1 and 880.7, corresponding to those of the ligand monomer (M^-, calculated *m*/*z* 440.1) and dimer ($(2M)^-$, calculated *m*/*z* 880.7) (see Supporting Information, Figure S7A). A third peak corresponding to a ligand trimer can also be seen. The peak of the dimer is verified by MS/MS (Figure S7B), with the signal of the monomer at *m*/*z* 440.4. Ligand pairing is also observed in mass spectrometry of the larger triazine-based ligand HTB, as demonstrated in an earlier communication.[10]

Syntheses. The assembly of metal ions or clusters and organic ligands into metal−organic frameworks can be regarded as a programmed system in which the steric and interaction information stored in the ligands is read by the metal ions through the algorithm defined by their coordination geometry.[25] It is key to select or design a suitable organic ligand to construct open MOFs possessing a desired topology. Considering that the chiral (10,3)-a net is a common structural type for MOFs containing planar BTC but that there are no such examples reported with nonplanar BTB as a ligand, it should be possible to construct open metal−organic frameworks with chiral channels by use of the planar TATB ligand. The likely presence of metastable chiral ligand-pair arrangements in solution (vide supra) increases the likelihood that chiral networks may result from such a synthesis. Thus, the solvothermal reaction between TATB and zinc or cadmium ions results in the formation of two open MOFs (**1** and **2**) possessing (10,3)-a nets with large chiral channels and hourglass SBUs with two terminal aqua ligands. However, compounds **1** and **2** are thermally unstable due to the easy removal of these aqua ligands from the SBU, leaving two-thirds of the metal ions in an unstable coordination environment.

To improve the stability of an open MOF, one may apply secondary building unit (SBU) stabilization or framework catenation.[7,26] Catenations depend on many factors and are largely unexplored. Previously reported work from this laboratory has demonstrated stable MOFs with framework

(21) (a) Johnson, E. R.; Wolkow, R. A.; DiLabio, G. A. *Chem. Phys. Lett.* **2004**, *394*, 334. (b) Sato, T.; Tsuneda, T.; Hirao, K. *J. Chem. Phys.* **2005**, *123*, 104307/1. (c) Zhao, Y.; Truhlar, D. G. *J. Phys. Chem. A.* **2005**, *109*, 4209.
(22) Jessiman, A. S.; MacNicol, D. D.; Mallinson, P. R.; Vallance, I. *J. Chem. Soc., Chem. Commun.* **1990**, 1619.
(23) (a) Thalladi, V. R.; Boese, R.; Brasselet, S.; Ledoux, I.; Zyss, J.; Jetti, R. K. R.; Desiraju, G. R. *Chem. Commun.* **1999**, 1639. (b) Thalladi, V. R.; Brasselet, S.; Weiss, H.-C.; Blaeser, D.; Katz, A. K.; Carrell, H. L.; Boese, R.; Zyss, J.; Nangia, A.; Desiraju, G. R. *J. Am. Chem. Soc.* **1998**, *120*, 2563. (c) Zyss, J.; Brasselet, S.; Thalladi, V. R.; Desiraju, G. R. *J. Chem. Phys.* **1998**, *109*, 658.
(24) Fujita, M.; Oguro, D.; Miyazawa, M.; Oka, H.; Yamaguchi, K.; Ogura, K. *Nature* **1995**, *378*, 469.
(25) (a) Hong, M.; Su, W.; Cao, R.; Fujita, M.; Lu, J. *Chem.*—Eur. J. **2000**, *6*, 427. (b) Lehn, J. M. *Supramolecular Chemistry-Concepts and Perspectives*; Wiley-VCH: Weinheim, Germany, 1995.

Table 2. Selected Interatomic Distances and Angles for **1**−**4**

param	**1**	**2**	**3**	**4**
space group	$P4_332$	$P4_332$	$P4_322$	$P4_322$
M2−O (Å)	1.98(2)	2.23(3)	1.962(5)	2.198(5)
M1−O (Å)	2.073(2)	2.32 (2)	2.077(6)	2.259(3)
triazine ring−benzene ring dihedral angle (deg)	*8.3*	*8.9*	*9.5*	*11.5*
Piedfort unit spacing d (Å) (plane-to-plane)	3.410	3.499	3.383	3.362
Piedfort unit rotational angle θ (deg)	30.6	27.9	30.5	30.0
M1···M2 (Å)	3.562	3.664	3.524	3.506
4_3 channel size (Å) (atom to atom)	13.14	13.44	12.40	12.76
triangular channel size (Å) (atom to atom)	20.93	21.23	a	a
calcd solvent-accessible vol (%)	79.2	80.0	54.6	55.0

[a] The triangular channels in **3** and **4** are subdivided into smaller channels by the infinite helices generated by formate or acetate linkers.

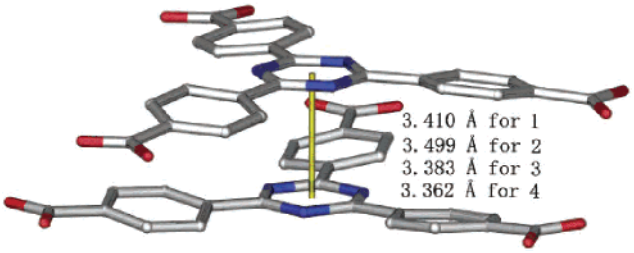

Figure 2. TATB D_3-Peidfort units, including ligand−ligand distances of **1**−**4**.

catenation through $\pi-\pi$ stacking; [10,11] the work herein pursues the alternate strategy of increasing stability of open MOFs with small labile ligands by SBU stabilization, as frameworks **1** and **2** already possess stacked ligand units and the catenation route to stabilization is unavailable. The labile aqua ligands can be replaced by formate or acetate generated in situ, connecting the hourglass SBUs to give rise to the one-dimensional helical chains found in **3** and **4**.

Frameworks 1 and 2. Reaction of H_3TATB with $M(NO_3)_2$ under solvothermal conditions results in formation of isostructural MOFs **1** (M = Zn) and **2** (M = Cd). Generally speaking, each of these MOFs is a non-interpenetrated (10,3)-a network with chiral 4_3 (or 4_1) and 2_1 channels along three orthogonal directions. Each compound forms as a racemic mixture of discrete $P4_332$ and $P4_132$ crystals; ensuing discussion will focus solely on 4_3 enantiomorphs.

In these structures, TATB ligands are nearly planar, with dihedral angles between central and peripheral rings less than 10° (Table 2). A D_3-Piedfort pair structure is evident, with stacked ligands separated by less than 3.5 Å (*d*) and offset with a rotational angle of ∼30° (θ), shown in Figure 2. Each D_3-Piedfort unit connects three trimetallic "hourglass" SBUs. In the hourglass SBU, shown in Figure 3, there are two peripheral metal atoms (labeled M2) tetrahedrally coordinated to three carboxylate oxygen atoms and one aqua ligand each, with the central third metal (M1) octahedrally coordinated to six carboxylate oxygen atoms (Figure 3). This arrangement

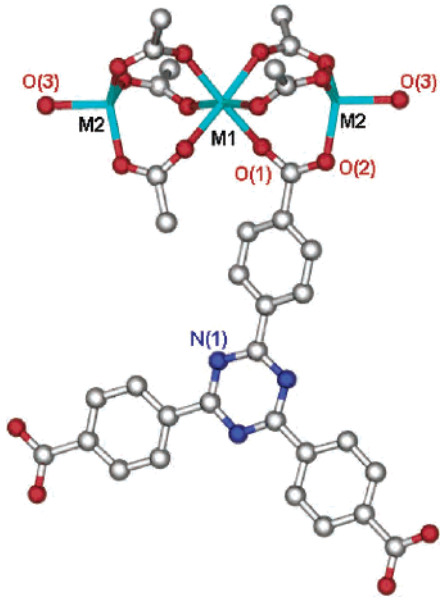

Figure 3. Coordination environment of metal ions in **1** (M = Zn) and **2** (M = Cd).

is uncommon but not unknown in reported literature;[27] however, **2** is the first example of Cd existing in a four-coordinate arrangement in a high-dimensionality framework. Six- to eight-coordinate modes are more typical for Cd in such networks.[28]

Every chiral ligand pair is bound to three SBUs in a left- or right-handed arrangement (Figure 4a), and every chiral SBU is bound to three ligand pairs in a fac arrangement to form a left- or right-handed propeller (Figure 4b). Both the TATB pairs and the propeller-type arrangement about each SBU are responsible for inducing chirality in the channels. The hourglass SBU is highly compatible with the D_3 mode of ligand stacking; the metal atoms hold the carboxylate "handles" to maintain a stacking angle of ∼30°. This strategy has been demonstrated with cocrystallized moieties which hold "handles" through hydrogen bonding[29] but rarely by strong metal−ligand bonds as found in **1** and **2**. Further evidence for SBU-enforced geometry comes from closer examination of the Piedfort pair shown in Figure 4b; the

(26) (a) Kitaura, R.; Iwahori, F.; Matsuda, R.; Kitagawa, S.; Kubota, Y.; Takata, M.; Kobayashi, T. C. *Inorg. Chem.* **2004**, *43*, 6522. (b) Batten, S. R.; Robson, R. *Angew. Chem., Int. Ed.* **1998**, *37*, 1460. (c) Rosi, N. L.; Eddaoudi, M.; Kim, J.; O'Keeffe, M.; Yaghi, O. M. *Angew. Chem., Int. Ed.* **2002**, *41*, 284. (d) Reineke, T. M.; Eddaoudi, M.; Moler, D.; O'Keeffe, M.; Yaghi, O. M. *J. Am. Chem. Soc.* **2000**, *122*, 4843. (e) Robson, R. *J. Chem. Soc., Dalton Trans.* **2000**, 3735. (f) Yaghi, O. M.; Li, H.; Davis, C.; Richardson, D.; Groy, T. L. *Acc. Chem. Res.* **1998**, *31*, 474.

(27) (a) Chen, W.; Wang, J. Y.; Chen, C.; Yu, Q.; Yuan, H. M.; Chen, J. S.; Wang, S. N. *Inorg. Chem.* **2003**, *4*, 944. (b) Clegg, W.; Little, I. R.; Straughan, B. P. *Inorg. Chem.* **1988**, *27*, 1916.

(28) Wu, C.-D.; Lin, W. *Chem. Commun.* **2005**, 3673.

(29) Sokolov, A. N.; Friščić, T.; MacGillivray, L. R. *J. Am. Chem. Soc.* **2006**, *128*, 2806.

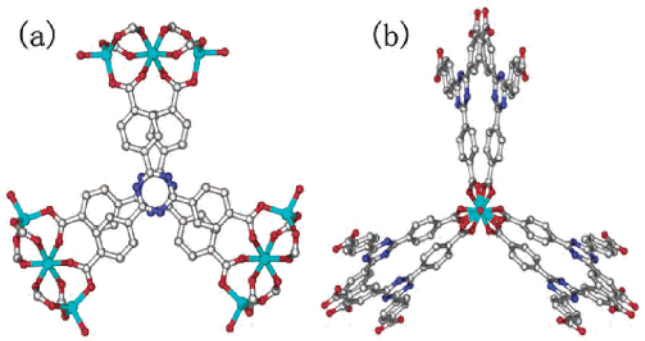

Figure 4. For **1** and **2**, a view of (a) TATB connecting three hourglass SBUs in a right-handed arrangment and (b) a left-handed propeller arrangment about an SBU.

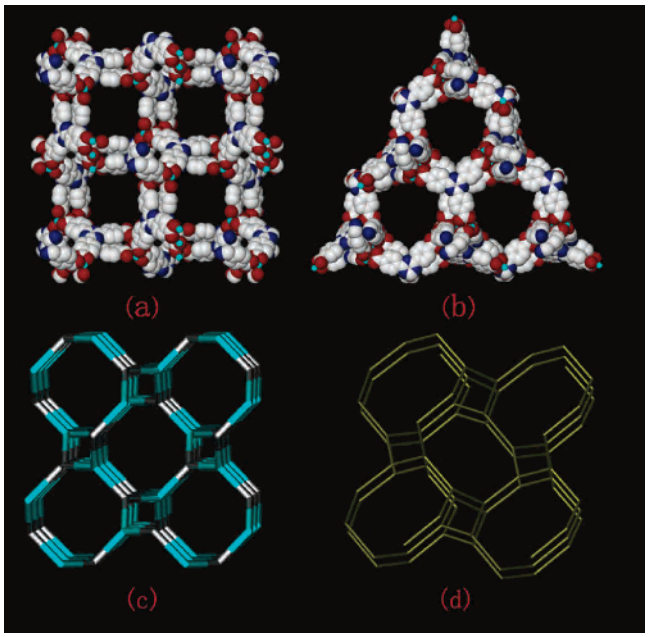

Figure 5. (a) 4_3 helical channels, viewed along the *b*-axis, (b) triangular mesochannels, viewed along [111], (c) the chiral (10,3)-a net of **1** and **2**, and (d) the Si net of the $SrSi_2$ structure.

ends of the TATB ligands are "pinched together" at the SBU to meet the metal atom coordination requirements. Clearly, the energetic penalty for deforming the ligand dimer from its equilibrium parallel-planes arrangement is compensated by the fulfillment of the metal coordination spheres through the formation of the hourglass SBU. The chiral propellers thus formed, as shown in Figure 4, propagate the chirality of the D_3-Piedfort unit throughout the network.

Compounds **1** and **2** are isostructural, with networks containing non-interpenetrating (10,3)-a nets in the well-known topology of the Si net of the $SrSi_2$-type structure (Figure 5). X-ray diffraction studies of **1**−**4** produced Flack parameters with values close to zero (see Table 2) implying high enantiopurity in single crystals. The idealized (10,3)-a net is constructed of bonds of equal length with uniform bond angles of 120° to create the 3-connected analogue of the 4-connected diamond net (Figure 5d), consisting of channels possessing 4_3 (or 4_1 in the other enantiomorph) and 2_1 symmetry along three orthogonal directions.

MOFs **1** and **2** are insoluble in common organic solvents and water and quickly become opaque when exposed to air due to solvate loss. Each contains very large chiral channels and a high solvent-accessible pore volume. 4_3 helical channels of 13.14 or 13.44 Å across (including van der Waals radii) extend in the [010] direction (Figure 5a), and triangular mesochannels with sides measuring approximately 20.93 or 21.23 Å extend in the [111] direction (Figure 5b) for **1** and **2**, respectively. Each network has a solvent-accessible volume of 79% or greater, as calculated by the PLATON suite.[14] Individual channel sizes and solvent-accessible volumes are summarized in Table 2. The N_2 sorption measurements of **1**, performed at 77 K, yielded a Langmuir surface area of 1100 m^2/g. However, MOF **2** does not retain its framework integrity after solvate removal, possibly due to the instability of low-coordinate Cd. Both **1** and **2** lack thermal stability because the coordinated water molecules on the SBUs are easily removed at elevated temperatures, resulting in unstable frameworks.

Generation of Functionality and Increased Stability. To improve the thermal stability of **1** and **2**, destabilization of the metal ion by labile ligand loss must be prevented. If the two labile aqua ligands in the hourglass SBU are replaced by nonlabile bridging ligands, the discrete SBUs will be connected to form an infinite chain of linked SBUs, which will in turn improve the stability of the SBU and the whole framework. To accomplish this, an attempt was made to use formate as a two-connected linker by adding sodium formate directly to the reaction mixture of **1**. Unfortunately, only an uncharacterized precipitate was obtained. However, an alternative method was devised on the basis of the knowledge that *N*,*N*-dimethylformamide (DMF) can decompose to release formate and dimethylamine slowly at high temperatures and/or under acidic conditions.[30] Therefore, several drops of HBF_4 were added to the original reaction mixture in the preparation of **1**. As a result, formate was generated in situ, connecting adjacent SBUs (see Supporting Information, Scheme S2) to form the one-dimensional 4_3 left-handed (or 4_1 right-handed) infinite helical chains observed in **3**. These helical chains are linked by achiral TATB ligands to produce a chiral three-dimensional porous framework.

As an extension of the method devised in the synthesis of **3** from **1**, an attempt was made to apply the same findings to the stabilization of **2**. Although **2** can be successfully obtained using DMF as the solvent, a crystalline product could not be isolated when HBF_4 was added to the reaction mixture used in the original preparation of **2**, and only an unknown precipitate resulted. The reasons for the lack of success with DMF are unclear; however, when *N*,*N*-dimethylacetamide (DMA) was used as the solvent, acetate ions were generated via catalysis by HBF_4 and **4** was isolated.

It should also be noted that **3** can alternately be synthesized from **1** (in a two-step process rather than a one-pot reaction). A reaction tube containing **1** and the accompanying solvent and reaction residues was opened, and several drops of HBF_4

(30) (a) Burrows, A. D.; Cassar, K.; Friend, R. M. W.; Mahon, M. F.; Rigby, S. P.; Warren, J. E. *Cryst. Eng. Commun.* **2005**, *7*, 548. (b) He, J.; Yu, J.; Zhang, Y.; Pan, Q.; Xu, R. *Inorg. Chem.* **2005**, *44*, 9279.

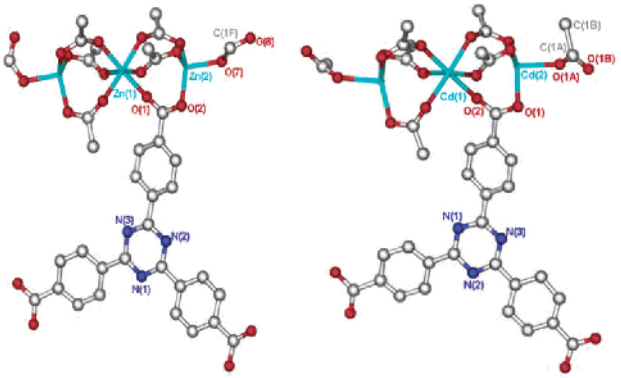

Figure 6. Coordination environment of metal ions in **3** (left) and **4** (right).

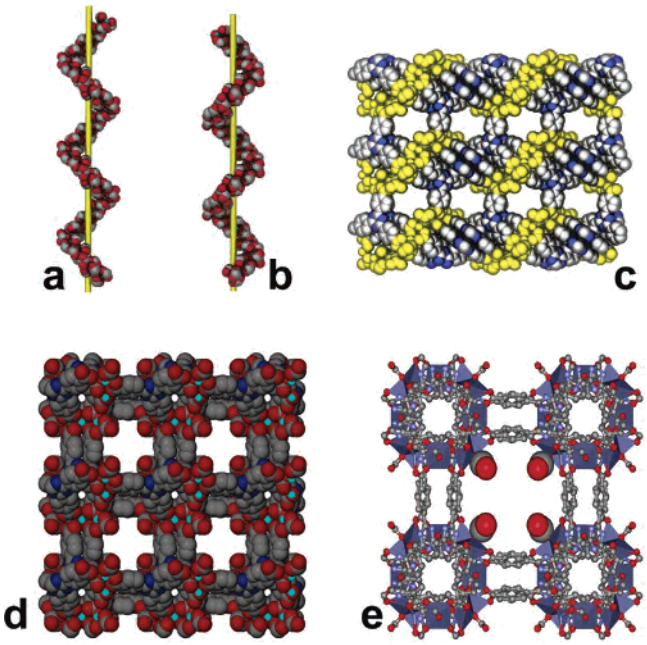

Figure 7. One-dimensional (a) left-handed and (b) right-handed helical chains generated by SBU threading in **3** and **4**, three-dimensional porous framework created by bridging helical chains (yellow) with TATB ligands (gray and blue) shown along the (c) *a*-axis and (d) *c*-axis, and (e) a functionalized chiral channel.

were added. A white precipitate was immediately observed. The tube was resealed under vacuum and heated to 120 °C for 24 h, resulting in colorless rodlike crystals of **3**.

Frameworks 3 and 4. Compounds **3** and **4** are 3D porous frameworks derived from **1** and **2**, respectively, with the terminally coordinated aqua ligands replaced by formate or acetate generated in situ (Figure 6); these compounds also crystallize as racemic mixtures of discrete $P4_122$ and $P4_322$ enantiomorphic crystals. Charge is localized in the formate or acetate, with C−O distances of 1.30(7) and 1.22(3) Å for formate in **1** and 1.28(3) and 1.17(2) Å for acetate in **2**. The carbonyl O atom bonds to two terminal metals on two adjacent hourglass SBUs (see Supporting Information, Scheme S2); the infinite helices thus generated interrupt the triangular channels found in **1** and **2**. MOFs **3** and **4** otherwise retain the same connectivity and basic framework motifs of the parent compounds **1** and **2**. Table 2 shows selected measurements for **3** and **4**.

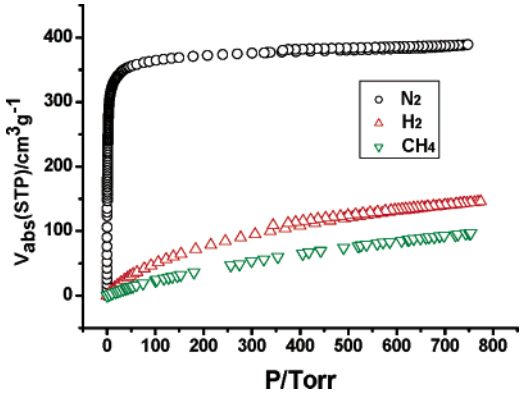

Figure 8. BET gas sorption isotherms of **3** at 77 K (N_2, H_2) and 195 K (CH_4).

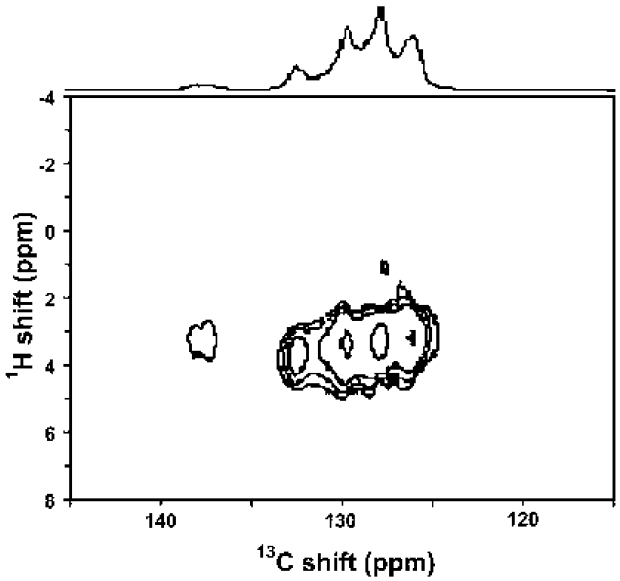

Figure 9. Two-dimensional $^{13}C/^1H$ HETCOR solid-state NMR for H_3-TATB.

One oxygen atom remains uncoordinated to metal ions, creating functionality in the chiral 4_1 or 4_3 channels of **3** and **4** and pointing toward the center of these channels to create hydrophilic voids (Figure 7) with dimensions in **3** of 9.053 × 9.053 Å between O atoms of formate groups and 12.40 × 12.40 Å between Zn atoms and in **4** of 8.809 × 8.809 Å between oxygen atoms of acetate groups and 12.76 × 12.76 Å between Cd atoms. As there is only one proton difference between dimethylamine and dimethylammonium, elemental analyses cannot distinguish between the presence of two dimethylamine molecules or one dimethylamine and one dimethylammonium ion. The presence of both an acid (acetic or formic) and a base (dimethylamine) of significant strengths led us to believe that the uncoordinated O atom should be deprotonated, creating anionic channel walls, with dimethylammonium ($[H_2N(CH_3)_2]^+$) counterions, along with free dimethylamine, DMA or DMF, and water molecules residing within the channels. This charge assignment is also in agreement with TGA studies and methane adsorption experiments (vide infra).

Thermal Stabilities of 1−4. TGA studies were carried out for **1**−**4**. MOF **1** shows a 27.7% weight loss from 50 to 430 °C, corresponding to the loss of eight water molecules

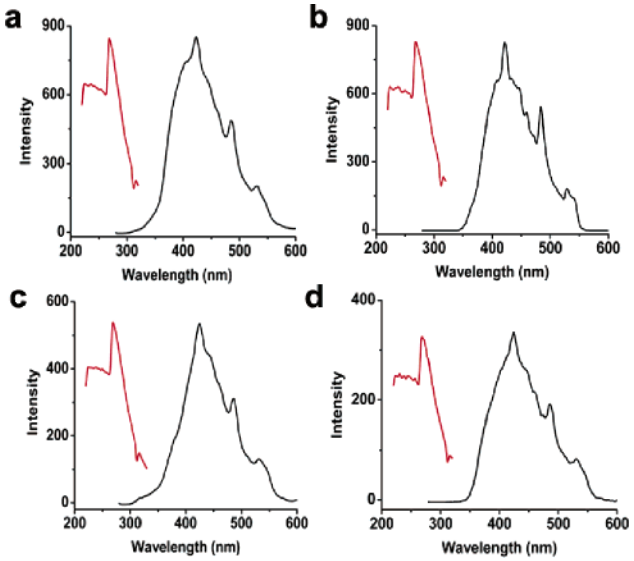

Figure 10. Excitation (red) and emission (black) spectra of (a) **1**, (b) **2**, (c) **3**, and (d) **4** in the solid state.

(including two coordinated aqua ligands) and four DMF solvates (calcd: 28.9%). The first weight loss for **2** is 21.5% from 60 to 120 °C, corresponding to the loss of ten free water and three DMA solvate molecules (calcd: 21.6%). MOF **2** also has a second weight loss of 18.5% from 120 to 200 °C, corresponding to the loss of four DMA solvates and two coordinated aqua ligands (calcd: 18.8%), with no further weight loss from 200 to 400 °C. High thermal stability was also found in **3**, with a weight loss of 19% from 45 to 255 °C, corresponding to the loss of three water, one dimethylamine, and three DMF solvate molecules (calcd: 20.5%), with no further weight loss above 255 °C. At temperatures above 410 °C, **3** begins decomposition. In **4**, the weight loss of 22% from 60 to 230 °C is the loss of three DMA, one dimethylamine, and four water molecules (calcd: 22.3%), with no further weight loss from 230 to 390 °C. Note that only one dimethylamine is lost upon heating, not two, further supporting that a dimethylammonium counterion exists within anionic channels.

Adsorption Properties. With an increasing desire to use MOFs in storage applications, gas and solvent adsorption were measured for MOFs **1**−**4**. In **1**, a type-I isotherm is observed for N_2 at 77 K, with a Langmuir surface area of 1100 m^2/g, indicating permanent porosity. Detailed adsorption measurements focus on **3** due to its high thermal stability.

Figure 8 shows the isotherms of **3** at 77 K for nitrogen and hydrogen and 195 K for methane. The H_2 sorption mass of **3** at 1 atm is 13 mg/g (1.3%), corresponding to a hydrogen storage density of 11.7 mg/cm^3, comparable to other reported values;[31] at this temperature and pressure the system is far from saturated. The measurement of methane adsorption at 195 K and 1 atm shows that **3** has an adsorption capacity of 4.3 mmol/g, corresponding to 69 mg/g. Though the channels of **3** are nanoporous, large enough to contain methane molecules, the methane adsorption volume is much lower than that of hydrogen. A possible explanation is that channels in **3** are anionic (vide supra) and less compatible with neutral and hydrophobic methane molecules than the more easily polarized dihydrogen molecules.

Reversible Adsorption. As-synthesized **3** was soaked with MeOH to remove DMF solvates from the pores and then dried under vacuum overnight to produce a solvent-free **3′**. TGA of **3′** indicates no weight loss from 45 to 410 °C. Samples of **3′** were placed in vapor diffusion chambers overnight with H_2O, MeOH, or $CHCl_3$, respectively. TGA measurements indicate that the pores of **3′** adsorb H_2O, MeOH, and $CHCl_3$, with respective formulas of $[H_2N(CH_3)_2][Zn_3(TATB)_2(HCOO)]\cdot 11H_2O$, $[H_2N(CH_3)_2][Zn_3(TATB)_2(HCOO)]\cdot 7MeOH$, and $[H_2N(CH_3)_2][Zn_3(TATB)_2(HCOO)]\cdot 2.5CHCl_3$. These solvent-saturated samples were regenerated to solvent-free samples by solvent exchange followed by heating under vacuum, and vapor diffusion experiments were repeated, demonstrating the reversible adsorption properties of **3**. The N_2 sorption at 77 K for **3** was examined, and a type-I isotherm was observed with a Langmuir surface area of 1558 m^2/g. This surface area is much higher than that of a known MOF containing chiral channels, $Ni_3(BTC)_2(3\text{-pic})_6(1,2\text{-pd})_3$.[5] The micropore volume based on BJH is 0.60 mL/g, corresponding well with the estimation of 54.6% solvent accessible volume calculated using PLATON[14] (based on the refined crystal structure and an estimated density of 0.90 g/mL.)

Solid-State NMR Spectra of 3. Multiple ^{13}C resonance peaks corresponding to carbons c and d (see Supporting Information, Figure S8) indicate slightly different structural conformations of the TATB powder. However, only two peaks are observed for carbons b and e. The well-resolved ^{13}C resonance assignments correlate to the structures shown in the inserted plot of Figure S8. The addition of Zn metal induces a 1.5 ppm upfield shift, most likely due to the interaction of the Zn metal with the carbonyl group. The ^{13}C resonance peak at 175 ppm (Figure S8B) confirms the formate linkage in **3**; the peak at 163 ppm marked with an asterisk (Figure S8A) represents a spinning side band.

A two-dimensional $^{13}C/^{1}H$ HETCOR solid-state NMR experiment of H_3TATB (Figure 9) was also performed, showing low-intensity contour peaks for carbons b and e (when compared to carbons c and d), indicating that protons are not directly bound to carbons b and e. Conversely, the observance of large peaks in carbons c and d suggest that protons are directly bound to these carbon atoms. Thus, the two-dimensional solid-state NMR data confirms the above carbon assignments.

Photoluminescence Properties. Several recent studies have examined the luminescence properties of MOFs for potential applications as light-emitting diodes (LEDs).[32] On the basis of current research of luminescent MOFs, the emission of coordination networks can be assigned to a

(31) Rowsell, J. L. C.; Millward, A. R.; Park, K. S.; Yaghi, O. M. *J. Am. Chem. Soc.* **2004**, *126*, 5666.

(32) (a) Lee, E. Y.; Jang, S. Y.; Suh, M. P. *J. Am. Chem. Soc.* **2005**, *127*, 6374. (b) Lill, D. T. d.; Gunning, N. S.; Cahill, C. L. *Inorg. Chem.* **2005**, *44*, 258.

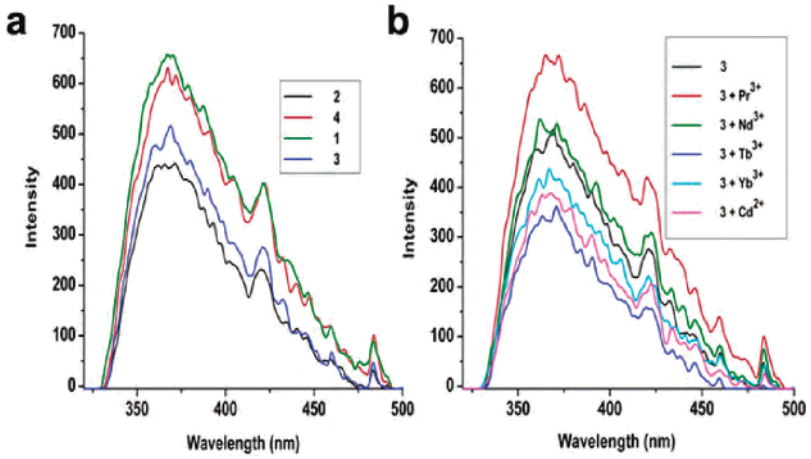

Figure 11. (a) Emission spectra of **1**−**4** in DMF suspensions (1×10^{-4} M). (b) Emission spectra of **3** after lanthanide or cadmium ion addition.

ligand-to-metal charge transfer (LMCT),[33] metal-to-ligand charge transfer (MLCT),[34] or an intraligand $\pi \rightarrow \pi^*$ transition. In general, metal coordination significantly influences fluorescence properties in MOFs (compared to organic ligands), an important property to consider when trying to synthesize new luminescent materials.

Photoluminescence measurements of **1**−**4** in the solid state at room temperature show that all four MOFs exhibit similar, strong luminescence at $\lambda_{max} = 423$, 422, 424, and 424 nm, respectively, upon excitation at 268.5 nm (Figure 10). The photoluminescent intensity of **1** and **2** is twice that of **3** and **4**. These emissions can be assigned to an intraligand $\pi \rightarrow \pi^*$ transition, as free TATB possesses a similar emission in the solid state ($\lambda_{max} = 423$ nm; see Supporting Information, Figure S11), though weaker than that of **1**−**4**.

It has been reported that a blue-shift in luminescence can occur in solution relative to that in the solid state,[35] as observed in this report. The maximum emission of TATB is 368.5 nm in solution, corresponding to a 54.5 nm blue-shift upon excitation at 268.5 nm. Luminescent intensity becomes weaker with increasing concentration (see Supporting Information, Figure S12). Perhaps a more interesting note is that a similar blue-shift is observed when MOFs **1**−**4** are suspended in DMF, in which the maximal blue-shifts are 56.0, 55.5, 63.5, and 56.5 nm, respectively (Figure 11a). Unlike for H_3TATB, the luminescent intensities of the MOFs become stronger with increasing concentration (Figure S13). This may result from solvent (DMF) quenching of H_3TATB; this quenching effect is absent in a suspension of a MOF.

The existence of anionic channels and high thermal stability prompted experiments adding lanthanide ions to **3**. The emission intensity of **3** increases significantly upon the addition of 3 equiv of Pr^{3+}. However, the addition of other lanthanide ions (Nd^{3+}, Tb^{3+}, Yb^{3+}) or cadmium (Cd^{3+}) leads to an unchanged or decreased luminescent intensity (Figure 11b). Therefore, **3** may have potential application as a selective luminescent probe for Pr^{3+}.

Second Harmonic Generation Property of 3. It is well-known that a noncentrosymmetric space group can be reflected by the second-harmonic generation (SHG) property. Preliminary SHG measurements of **3** corroborate the previously determined space group assignment. MOF **3** displays a SHG response in the powder state three times greater than that of urea, slightly stronger than some chiral MOFs constructed from chiral organic ligands.[36] This indicates that **3** may have potential applications in nonlinear optics.

Summary. Results and conclusions of these investigations are summarized as follows:

(1) The design of the triazine-based, trigonal-planar TATB ligand, which has a metastable chiral stacking mode, and the creation of "hourglass" SBUs, which are themselves chiral, allow the synthesis of MOFs 1−4 with large chiral channels of 20.93 and 21.23 Å in 1 and 2, respectively, and chiral, microporous channels of 12.40 and 12.76 Å in 3 and 4, respectively. These are among the largest chiral channels crystallographically characterized.

(2) By the connection of "hourglass" SBUs using formate or acetate in **3** or **4**, respectively, infinite helical chains form within the MOFs. This novel SBU stabilization strategy greatly increases the thermal stability and the framework stability of the MOFs after solvent removal and may have general implications in MOF preparation. TGA studies show that MOFs **3** and **4** are stable to 410 and 390 °C, respectively, record highs for MOFs containing chiral channels. The existence of carboxylate-linked SBU chains is confirmed by ^{13}C solid-state NMR, and high-temperature stability is confirmed by XRPD studies.

(3) Reversible adsorption is observed by TGA after vapor diffusion of **3′** with methanol, water, and chloroform, while N_2 sorption of **3′** at 77 K shows a type-I isotherm with a high Langmuir surface area of 1558 m^2/g. This reversible adsorption of water on a MOF is very rare.

(4) MOF **3** may have potential application as a selective luminescent probe for Pr^{3+}, and all four MOFs have potential

(33) Fu, Z.-Y.; Wu, X.-T.; Dai, J.-C.; Hu, S.-M.; Du, W.-X.; Zhang, H.-H.; Sun, R.-Q. *Eur. J. Inorg. Chem.* **2002**, *2002*, 2730.
(34) (a) Abedin-Siddique, Z.; Ohno, T.; Nozaki, K.; Tsubomura, T. *Inorg. Chem.* **2004**, *43*, 663. (b) Pope, S. J. A.; Coe, B. J.; Faulkner, S.; Bichenkova, E. V.; Yu, X.; Douglas, K. T. *J. Am. Chem. Soc.* **2004**, *126*, 9490.
(35) Sun, S. S.; Lees, A. J. *Chem. Commun.* **2002**, *230*, 171.
(36) (a) Anthony, S. P.; Radhakrishnan, T. P. *Cryst. Growth Des.* **2004**, *4*, 1223. (b) Qu, Z.-R.; et al. *Chem.*—Eur. J. **2004**, *10*, 53.

applications in LED technology. MOFs **1**−**4** exhibit strong luminescence at λ_{max} of 423, 422, 424, and 424 nm, respectively, upon excitation at 268.5 nm.

Herein we have demonstrated the use of building-block construction with ligand and SBU design to create functionalized MOFs with large chiral channels. Thermal stability and framework stability after guest removal have been improved by SBU stabilization without a significant concomitant sacrifice of porosity. In continuing these studies, we gain a more in-depth understanding of chiral MOF assembly using achiral components and hope to design new functionalized MOFs for a wide range of potential applications.

Acknowledgment. This work was supported by the National Science Foundation (Grant CHE-0449634), Miami University, and the donors of the American Chemical Society Petroleum Research Fund. H.-C.Z. also acknowledges the Research Corp. for a Research Innovation Award and a Cottrell Scholar Award. The diffractometer was funded by NSF Grant EAR-0003201 and used in cooperation with the Miami University Department of Geology. The 500-MHz wide-bore NMR spectrometer was obtained with NSF Grant CHE-0116333. We acknowledge Gengxin Zhang for assistance in collection of XRPD data, Jing-Lin Zuo for SHG measurements, Krishnan Damodaran for the collection of ^{13}C solid-state NMR data, Jianmin Li for help in computational chemistry, and Tracy M. Mattox for helpful discussion.

Supporting Information Available: Crystallographic information (CIF files) for all seven structuresm a MS spectrum of TATB, TGA data for **3** and **3′**, an XRPD of **3**, luminescence of TATB in the solid state and in DMF solution, excitation and emission spectra of **3** in DMF, IR spectra of TATB and MOFs **1**−**4**, further discussion of computational methods, and complete refs 19 and 36b. This material is available free of charge via the Internet at http://pubs.acs.org.

IC0624773